AXIAL DISTRIBUTION OF OPTICAL EMISSION IN A PLANAR MAGNETRON DISCHARGE

by

Lan Gu and M. A. Lieberman

Memorandum No. UCB/ERL M88/6

4 January 1988

AXIAL DISTRIBUTION OF OPTICAL EMISSION IN A PLANAR MAGNETRON DISCHARGE

by

Lan Gu and M. A. Lieberman

Memorandum No. UCB/ERL M88/6

4 January 1988

ELECTRONICS RESEARCH LABORATORY

College of Engineering
University of California, Berkeley
94720

AXIAL DISTRIBUTION OF OPTICAL EMISSION IN A PLANAR MAGNETRON DISCHARGE

by

Lan Gu and M. A. Lieberman

Memorandum No. UCB/ERL M88/6

4 January 1988

ELECTRONICS RESEARCH LABORATORY

College of Engineering
University of California, Berkeley
94720

Axial Distribution of Optical Emission in a Planar Magnetron Discharge

Lan Gu and M. A. Lieberman

Department of Electrical Engineering and Computer Sciences

and the Electronics Research Laboratory

University of California, Berkeley, CA 94720

ABSTRACT

We measure the axial distribution S of optical emission in a dc planar magnetron discharge for various currents I, voltages V and magnetic fields B. We develop an integral equation model of the distribution, which is in good agreement with the measurements. At fixed I, we find that the position Δ from the cathode of the peak in emission S_{max} scales as the ion Child law sheath thickness $\Delta \propto V^{7/8}/B^{1/4}$, and that for small B's, $S_{max} \propto B/V^{1/2}$.

I. INTRODUCTION

Planar magnetron discharges are widely used for thin film deposition in the electronics industry [1-3]. There have been a number of studies of the plasma properties of these discharges [4-7]. However a complete discharge model has still not been developed, and the relations among the discharge parameters are unclear. We have performed some experiments to study the properties of the cathode region and their variation with magnetic field strength, current and pressure.

A planar magnetron discharge is a low pressure, magnetic field enhanced, dc glow discharge. Typical operating conditions are pressures, 1-50 mtorr; magnetic fields, 100-500 G, current densities, 1-100 mA/cm^2, and voltages 200-700 V. The dc magnetic field is applied such that the field lines enter and leave through the cathode (target) plate. Under these conditions, most of the applied voltage is dropped across a thin sheath near the cathode surface. Argon ions, unconfined by the magnetic field, are accelerated through the sheath into the cathode. In addition to sputtering target material, the ion bombardment produces secondary electron emission at the cathode. These electrons are accelerated back into the plasma and are trapped on the field lines, drifting azimuthally and electrostatically mirroring against the cathode plate. These trapped electrons produce a sufficient ionization to maintain the discharge. In cylindrically-symmetric geometry, the discharge appears as a bright ring, having mean radius r_o and mean radial thickness $\bar{w}$, which hovers a few millimeters above the cathode surface.

Our discharge apparatus is shown in Fig. 1. Two 9" diameter copper plates are mounted on the axis of a 12" diameter aluminum vacuum vessel. Each plate is water-cooled, insulated from the vessel, and can be moved along the axis. Seven 2" diameter parts in the plane of symmetry provide diagnostics access. The magnetic field is generated by a cylindrically symmetric electromagnet carrying a current I_M. The field shape near the cathode surface is shown in Fig. 2. The radius r_0 where the field B is tangent to the cathode surface is approximately 5 cm from the axis. We quote values of B on the cathode plate at r_0 in the following discussion, where $B \approx 28.5$ gauss per ampere of magnet current.

The most obvious characteristic of a low pressure, planar magnetron discharge is its current-voltage relation and the low discharge voltage, as compared to a non magnetic field- enhanced, dc glow discharge at the same pressure and current. Figure 3 shows I versus V for our discharge as the mag-

netic field is increased, illustrating this transition from glow to magnetron operation. At a fixed I, V decreases as B is increased. We can understand this transition as follows: without a magnetic field in the vicinity of the cathode surface, secondary electrons emitted by ion bombardment of the cathode accelerate into the plasma with a large ionization mean free path and move from the cathode to the anode, producing few electron-ion pairs. When the magnetic field is present, then these electrons are trapped on the field lines. This yields a greatly enhanced production of electron-ion pairs, which suffices to maintain the discharge at a much lower voltage than occurs in the absence of the confining magnetic field.

II. OPTICAL EMISSION MEASUREMENTS

In order to measure the axial distribution $S(z)$ of optical emission near the cathode surface, we used a photomultiplier tube detector with a lens and a collimator consisting of two apertures and a cylinder blackened in its interior, having inner diameter 3/8" and length 7.5". A micrometer was mounted on a chamber port to move the collimator along the chamber axis, with the collimator axis held parallel to the cathode surface. The system is shown in Fig. 4.

The axial resolution of the system was measured using an illuminated ground glass slot set in the port window opposite to the port holding the collimator. The measurement yielded a resolution of 0.28 mm along the axis of the chamber.

Measurements of S for the planar magnetron discharge were made for various magnetic field strengths, discharge currents and pressures. Typical results are shown in Fig. 5. The general behavior is as follows: As the distance z from the cathode surface is increased, the emission rises sharply to a first peak, falls slightly, rises to a large second peak, and then slowly falls. The small first peak, which is 0.2-0.4 mm from the cathode surface, was identified as an artifact due to diffuse reflection of light from the cathode surface. This was verified using a lamp to illuminate the cathode, producing a similar effect. When the cathode was covered with a blackened surface, this first peak disappeared.

In a low pressure magnetron discharge, the sheath region near the cathode is particularly important. We have examined whether the second large peak in S, 2-8 mm from the cathode surface, is associated with the sheath-plasma boundary. We measured the position Δ of this peak from the cathode

for various discharge currents, pressures and magnetic field strengths, concentrating on the variation of Δ with B. These data for fixed I and p are shown as the "stars" in Figs. 6a-c. We see that Δ decreases with increasing magnetic field B. At the same time, as shown in Fig. 3, the discharge voltage V decreases as B increases.

There are two possible characteristic distances relevant to the position Δ of the observed peak: (1) The peak might be associated with the energetic electron gyroradius $\lambda = u/\omega$, where u is the energetic electron velocity and ω is the electron gyration frequency. Using $u = (2eV/m)^{1/2}$ and $\omega = eB/m$, we obtain

$$\lambda = \left[\frac{2m}{e}\right]^{1/2} \frac{V^{1/2}}{B} . \tag{1}$$

(2) The position of the peak may be associated with the mean (with respect to radius) Child's law sheath thickness d, defined by

$$\bar{J}_i = \frac{4\varepsilon_0}{9} \left[\frac{2e}{M}\right]^{1/2} \frac{V^{3/2}}{d^2} \tag{2}$$

where $\bar{J}_i \simeq J_{ipeak}/2$ is the mean ion current density of the current distribution at the cathode, and M is the ion mass (argon). Solving for d, we obtain

$$d = \frac{2}{3} \varepsilon_0^{1/2} \left[\frac{2e}{M}\right]^{1/4} \frac{V^{3/4}}{\bar{J}^{1/2}} . \tag{3}$$

We see that both λ and d decrease as B increases (because V decreases also).

Measurements of the radial ion current profile at the cathode (for the data of Fig. 6a only) show that the mean width at half-maximum $\bar{w}$ decreases as the magnetic field is increased. Both a theoretical model of the distribution and the measurements indicate that $\bar{w} \simeq (2a\,\lambda)^{1/2}$ where a is the magnetic field line curvature of the field line tangent to the plate at $r = r_0$ [7]. The mean area $\bar{A}$ of the discharge is then

$$\bar{A} = 2\pi r_0 \bar{w} . \tag{4}$$

with

$$I = 2\pi r_0 \bar{w} J_{ipeak} \ . \tag{5}$$

Using (4) and (5) in (3) we obtain

$$d = \frac{4\sqrt{2}}{3} (\pi r_0 \varepsilon_0)^{1/2} \left[\frac{e}{M}\right]^{1/4} \left[\frac{2m}{e}\right]^{1/8} \frac{a^{1/4} V^{7/8}}{I^{1/2} B^{1/4}} \tag{6}$$

for a fixed I.

Using measured values of I, V, B, and $\bar{w}$, the gyroradius (1) is plotted as the solid line in Figs. 6a-c, and the Child law sheath thickness (6) is plotted as the dashed line. Although the position Δ of the measured peak in optical emission is typically a factor of two larger than the Child's law thickness d, we observe qualitatively that the scaling of Δ with B agrees quite well with Child's law.

To test quantitatively whether Δ satisfies the scaling laws (1), (3), or (6), we plot versus B in Fig. 7 the three quantities $\Delta B/V^{1/2}$ [for Eq. (1)], $\Delta/V^{3/4}$ [for Eq. (3)] and $\Delta B^{1/4}/V^{7/8}$ [for Eq. (6)], for the data shown in Figs. 6a-c. At high currents (Fig. 7a and 7c), the best fit is to (6), Child's law including the proper scaling with mean current width $\bar{w}$. The quantity $\Delta B^{1/4}/V^{7/8}$ is constant within ± 8% over a factor of four variation in magnetic fields and a factor of two variation in voltage. Neglecting the scaling of $\bar{w}$ with B in Child's law yields a worse result. The scaling of Δ with gyroradius is clearly incorrect. At lower currents (Fig. 7b at 0.1 A) where $\lambda \leq d$ and at very high magnetic fields, some deviation from the scaling predicted by (6) is seen.

From the measured sheath thickness and the discharge voltage, we also can estimate the average electric field strength $\langle E \rangle \approx V/\Delta$ in the sheath. These values are shown in Table 1 for the data of Fig. 6a. $\langle E \rangle$ increases slightly as B is increased. We also give the drift velocity $u_E = \langle E \rangle / B$ and the azimuthal component $u = 2u_\phi/\pi$ of the energetic electron velocity u_0 in the table. For low magnetic fields such that $\lambda \gg d$, we expect that the electrons gyrate in semi-circular orbits as they reflect from the thin sheath region, spending most of their time in the field free region outside the sheath; their azimuthal drift velocity is then u_ϕ. For high magnetic fields such that $\lambda \ll d$, we expect that the electrons gyrate in a cycloidal motion within the sheath where the electric field $\langle E \rangle$ is present; the azimuthal drift velocity is then u_E. For commercial planar magnetron discharges used for thin film deposition, the magnetic field is generally small and the dc current is large. This regime is characterized by

$\lambda \gtrsim d$, such that the characteristic energetic electron azimuthal drift velocity is u_ϕ, not u_E. Finally, we note that the sheath thickness is small compared with the ion-neutral mean free path at low pressures: $\lambda_{mfp} \simeq 3$ cm at $p = 10$ mtorr.

III. OPTICAL EMISSION MODEL

In order to explain the observed axial optical emission $S(z)$ and the dependence of the axial position Δ of the peak emission on Child's law, we have developed a geometrical model of the planar magnetron ring discharge [7]. We model the transverse ion current distribution based on a simplified (two dimensional rectangular) field geometry (see Fig. 8) in which (a) the B-field is generated by current in a single wire running parallel to the plate (having half-width x_p) at a distance a below the surface (the field lines are circles); (b) the cathode sheath is infinitesimally thin, such that (fast) electrons leave the plate with kinetic energy $e\Phi$, where Φ is the discharge voltage; and (c) the electron motion is Hamiltonian in the effective potential bounded by the field lines, such that an electron emitted at x_0 ergodically explores the accessible phase space area $\tau(x_0)$. We let $h(x,x_0)dx$ be the phase space area explored by an electron emitted at x_0 which contributes to the ion current $J_i(x)$, γ be the secondary emission coefficient, and H be the total number of ionizations per fast electron. Then we arrive at an integral equation

$$J_i(x) = H\gamma \int_{-x_p}^{x_p} dx_0 \, \frac{h(x,x_0)}{\tau(x_0)} \, J_i(x_0) \tag{7}$$

which we solve numerically, yielding a distribution $J_i(x)$ that is peaked at x = 0 and has a mean width $\overline{w} \simeq (2\lambda a)^{1/2}$, where λ is the energetic electron gyroradius. Two types of regions $\tau(x_0)$ contribute to the integral in (7). For $x_0 > x_1 = (2\lambda a)^{1/2}$, τ is an arc-shaped region, as shown in Fig. 8a. For $x_0 < x_1$, τ is a wedge-shaped region, as shown in Fig. 8b. Since $J_i(x)$ is small for $x_0 > x_1 = \overline{w}$, the wedge-shaped regions for $0 < x_0 < x_1$ dominate the dynamics.

To determine the optical emission distribution $S_T(z)$ from the model, we integrate the contribution of all wedge-shaped regions to the light emitted along a line-of-sight l parallel to the cathode surface of a distance z above the surface (see Fig. 8b). Using $\tau = (x_0^2+x_1^2)^{-3/2}$ and $l = (x_0^2+x_1^2-2z)^{1/2}$, we obtain

$$S_T(z) \propto \int_{x_{min}}^{x_1} dx_0 J_i(x_0) \frac{(x_0^2+x_1^2-2z)^{1/2}}{(x_0^2+x_1^2)^{3/2}} \tag{8}$$

where

$$x_{min} = \begin{cases} 0, & 2z < x_1^2; \\ (2z-x_1^2)^{1/2}, & x_1^2 < 2z < 2x_1^2; \\ x_1, & 2z > 2x_1^2. \end{cases} \tag{9}$$

Figure 9 shows the normalized optical emission distribution $s_T(x) = S_T(x)/S_T(0)$ according to this model for a Gaussian current distribution $J_i(x_0) \propto \exp[-x_0^2/x_1^2]$. The results do not much depend on the exact shape of J_i; a rectangular shape cutoff at $x_0 = x_1$ yields a similar result (see Fig. 9).

Because the electrons only reach their full energy after acceleration across the Child's law sheath, the optical emission within the sheath due to electron-neutral excitation is assumed to be low. Therefore, the intensity distribution shown in Fig. 9 begins at the sheath edge as indicated in the figure. The theory predicts that the normalized optical emission distribution is a universal function of $\alpha = z/\lambda$. The data of Fig. 5 are generally in agreement with this prediction for $\alpha \lesssim 1$. However, for $\alpha \gtrsim 1$, the actual emission is higher than predicted, presumably due to diffusion of hot electrons or optical emission by cold electron excitation of neutrals.

To examine quantitatively the correspondence between the measured and theoretical optical emission, we plot in Fig. 10 the maximum value S_{max} (with respect to z) of the optical emission at fixed current versus the magnetic field B for p = 5 mtorr and p = 20 mtorr. We normalize these data to the maximum with respect to B, which occurs for 290 - 340 G at 5 mtorr and for 400 G at 20 mtorr. We see that S_{max} increases with B to a peak value at $B \approx B_{peak}$ and then falls slightly as B is increased above B_{peak}. We can understand the behavior of S_{max} in the regime $\lambda \gtrsim d$ from the emission model. At the sheath edge z = 0, from (8),

$$S_{T\,max} \propto \int_0^{x_0} dx_0 \frac{J_i(x_0)}{x_0^2+x_1^2} . \tag{10}$$

Letting $J_i(x_0) \propto I/x_1$ and integrating (10), we obtain $S_{T\,max} \propto I/x_1^2$. Since $x_1^2 = 2\lambda a$, we find that

$$S_{T\max} \propto I/\lambda \propto I B/V^{1/2} . \tag{11}$$

Using the data for λ versus B at a fixed I, we plot $1/\lambda$ versus B in Fig. 10. We see that $S_{T\max}$ does indeed scale with $1/\lambda$ for small B. The peak in $S_{T\max}$ may be associated with the condition $\lambda \sim d$, since for $\lambda > d$, the assumptions of the emission model are invalid.

We can estimate the axial (area-averaged) ionization efficiency $\eta'(x)$ of the discharge as follows:

$$\eta'(x) = \frac{e}{I} \left[\frac{dN'}{dt}\right]_{iz} , \tag{12}$$

where $(dN'/dt)_{iz}$ is the total number of electron-ion pairs created per second per unit axial length in the discharge. We expect $(dN'/dt)_{iz}$, and therefore $\eta'(x)$, to be proportional to $S(x)$, since the optical excitation frequency is roughly proportional to the ionization frequency for energetic electron collisions with gas atoms.

IV. CONCLUSIONS

We have measured the axial light emission near the cathode of a dc planar magnetron discharge over a range of pressures and magnetic fields, and we have compared these measurements to a simple model of the geometric structure of the ring-shaped discharge. The distance from the cathode to the peak value of light emission is identified as the ion Child's law sheath thickness. The shape of the axial distribution of light is in reasonable agreement with the model. The behavior of the peak value of light emission versus magnetic field strength also agrees with the model for low magnetic field strengths.

We gratefully acknowledge the assistance of H. Meuth and A.E. Wendt in carrying out these studies. This research was supported by National Science Foundation Grant ECS-8517363 and by a Gift from Varian Associates, Inc.

REFERENCES

[1] J. A. Thornton and A. S. Penfold, in *Thin Film Processes*, ed. by J. L. Vossen and W. Kern (Academic Press, New York, 1978), 76.

[2] R. K. Waits in *Thin Film Processes*, ed. by J. L. Vossen and W. Kern (Academic Press, New York, 1978), 131.

[3] J. A. Thornton, *J. Vac. Sci. Technol.* 15(2) March/April 1978.

[4] S. M. Rossnagel and H. R. Kaufman, *J. Vac. Sci. Technol. A* 4, 1882 (1986).

[5] H. Fujita, S. Yagura, H. Ueno and M. Nagano, *J. Phys. D: Appl. Phys.* 19, 1699 (1986).

[6] J. M. Rossnagel and H. R. Kaufman, *J. Vac. Sci. Technol. A* 5, 88 (1987).

[7] A. E. Wendt, M. A. Lieberman, and H. Meuth, "Radial Current Distribution at a Planar Magnetron Cathode," Electronics Research Laboratory Report, University of California, Berkeley, CA 94720; to appear in *J. Vac. Sci. Technol.* (1988).

TABLE 1

Discharge Parameters for I = 0.5 A and p = 5 mtorr

B (G)	V (V)	λ(mm)	Δ(mm)	d (mm)	E (V/cm)	E/B (10^8cm/s)	u_ϕ(10^8cm/s)
142	670	6.10	3.56	2.43	188.0	13.2	9.77
171	525	4.52	2.92	1.87	179.8	10.5	8.65
228	443	3.10	2.41	1.50	183.8	8.06	7.95
285	428	2.44	2.03	1.37	210.8	7.40	7.81
342	396	1.96	1.70	1.23	232.9	6.81	11.8
456	362	1.41	1.65	1.05	219.6	4.81	7.18
570	325	1.07	1.52	0.91	213.8	3.75	6.81

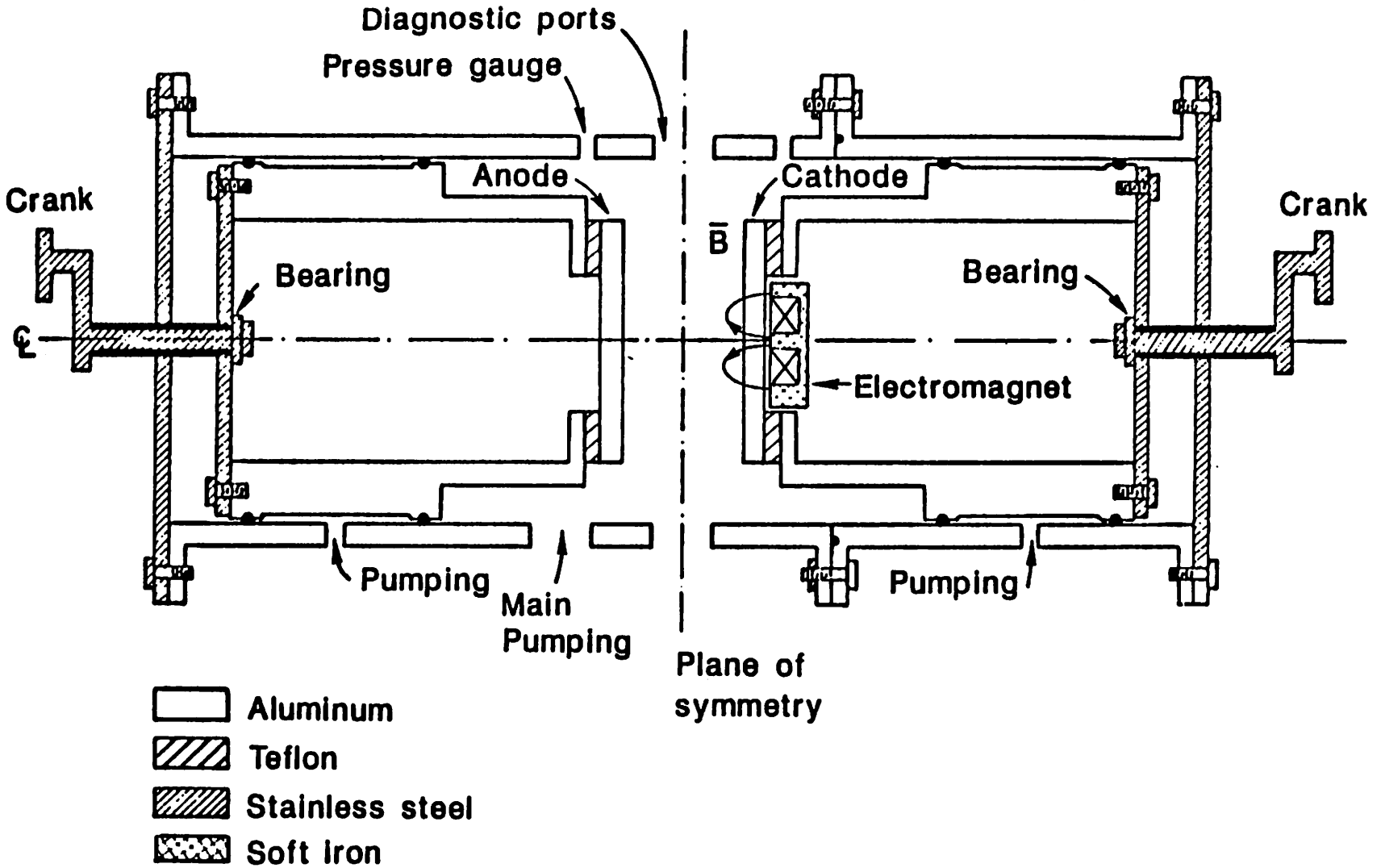

Fig. 1. Planar magnetron discharge experimental chamber.

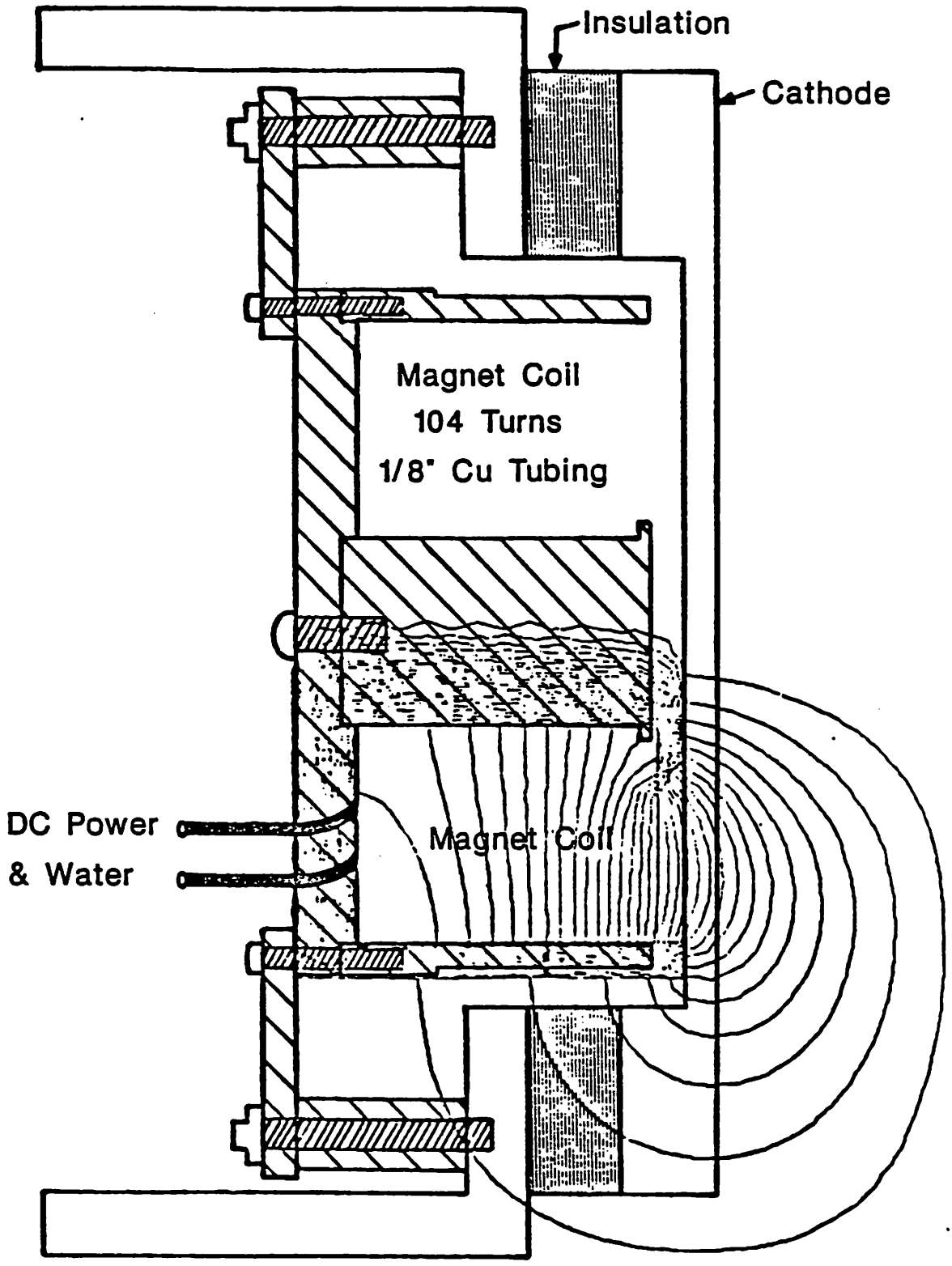

Fig. 2. Cross section of cathode configuration showing the magnetic field lines.

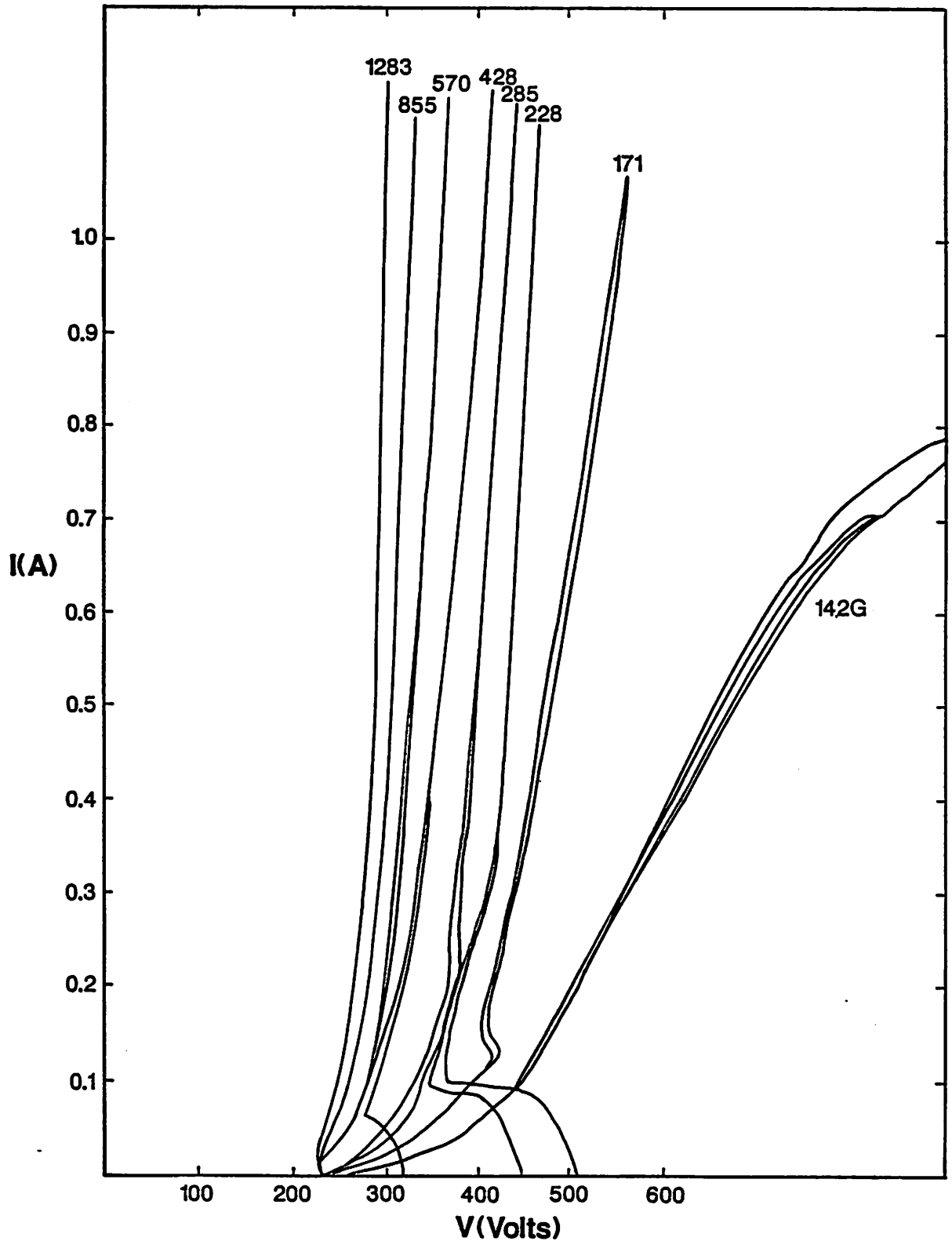

Fig. 3. Current I versus voltage V for various magnetic fields B, in 5 mtorr argon gas.

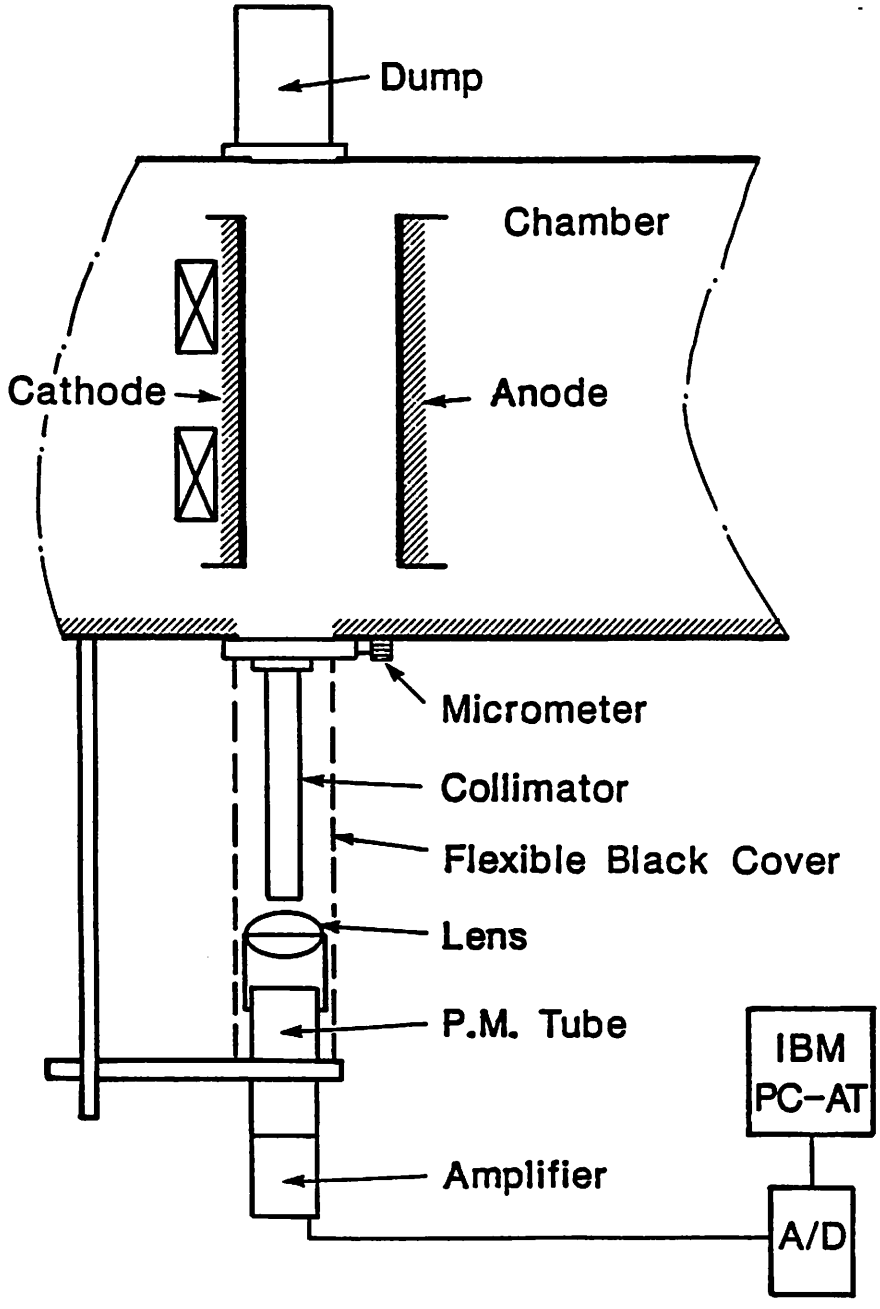

Fig. 4. Axially-resolved optical emission detector.

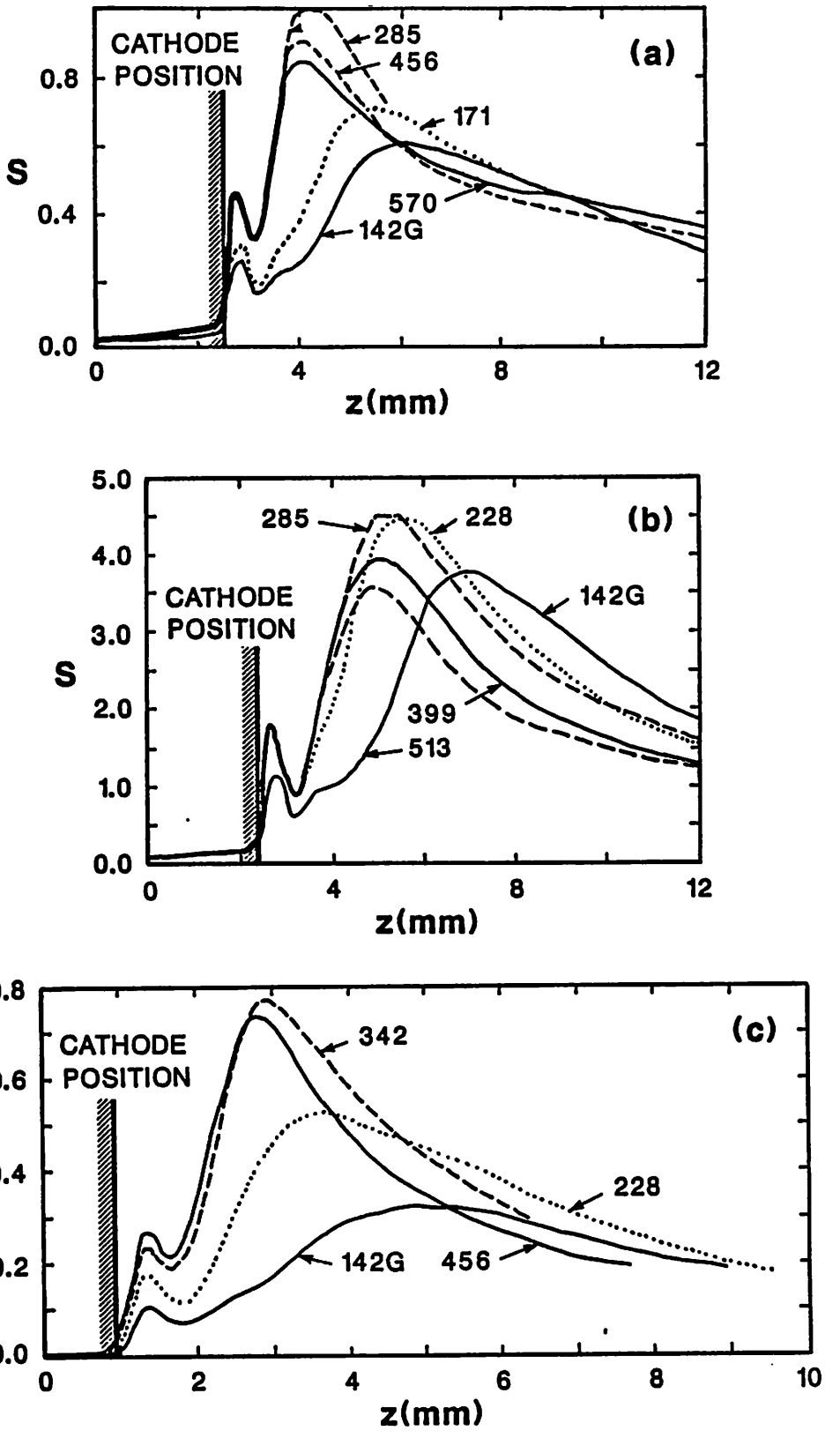

Fig. 5. Optical emission S versus axial distance z; (a) I = 0.5 A, p = 5 mtorr; (b) I = 0.1 A, p = 5 mtorr; (c) I = 0.5 A, p = 20 mtorr.

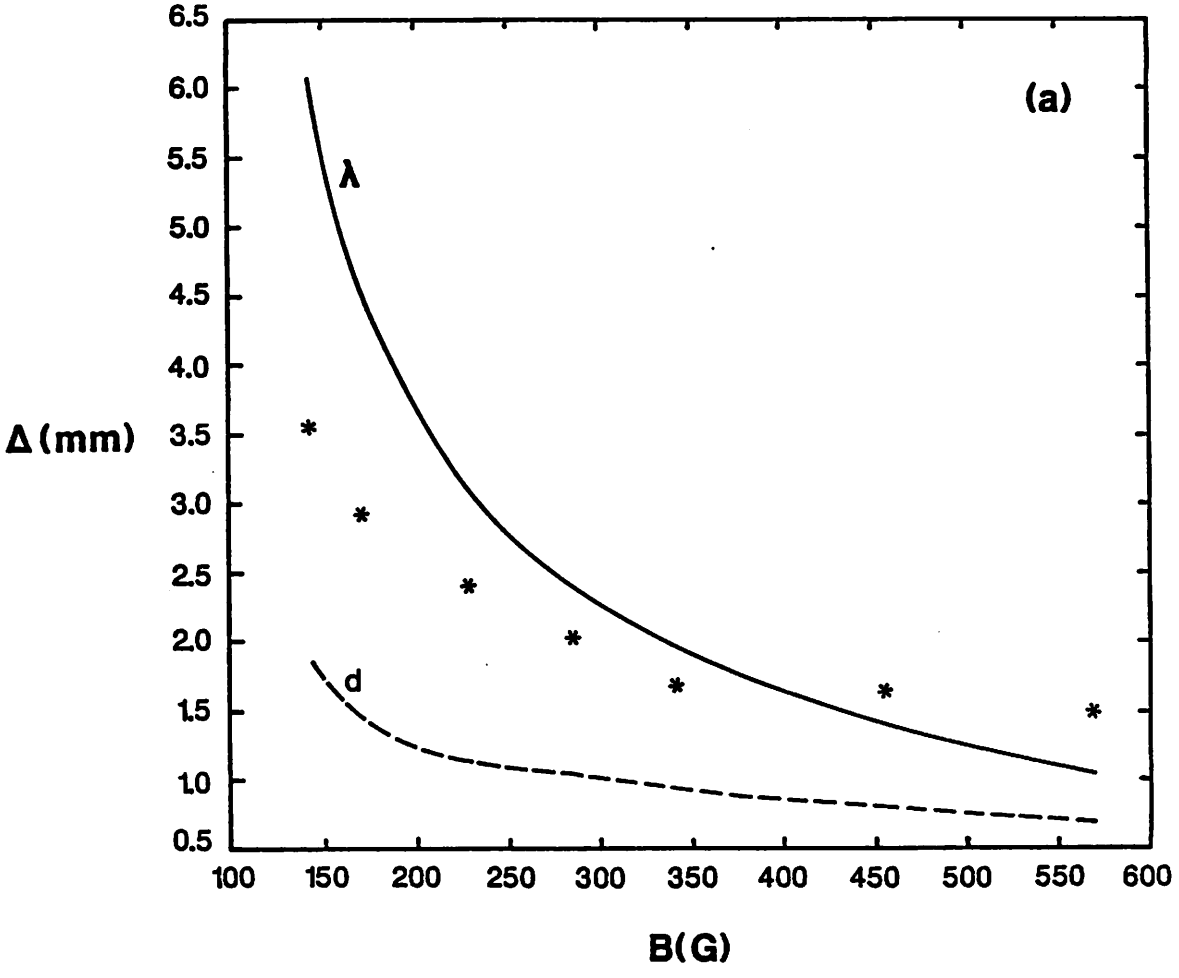

Fig. 6. Position Δ from the cathode of the peak in optical emission versus magnetic field B. For comparison, the gyroradius λ and the Child's law ion sheath thickness d are also shown; (a) I = 0.5 A, p = 5 mtorr; (b) I = 0.1 A, p = 5 mtorr; (c) I = 0.5 A, p = 20 mtorr.

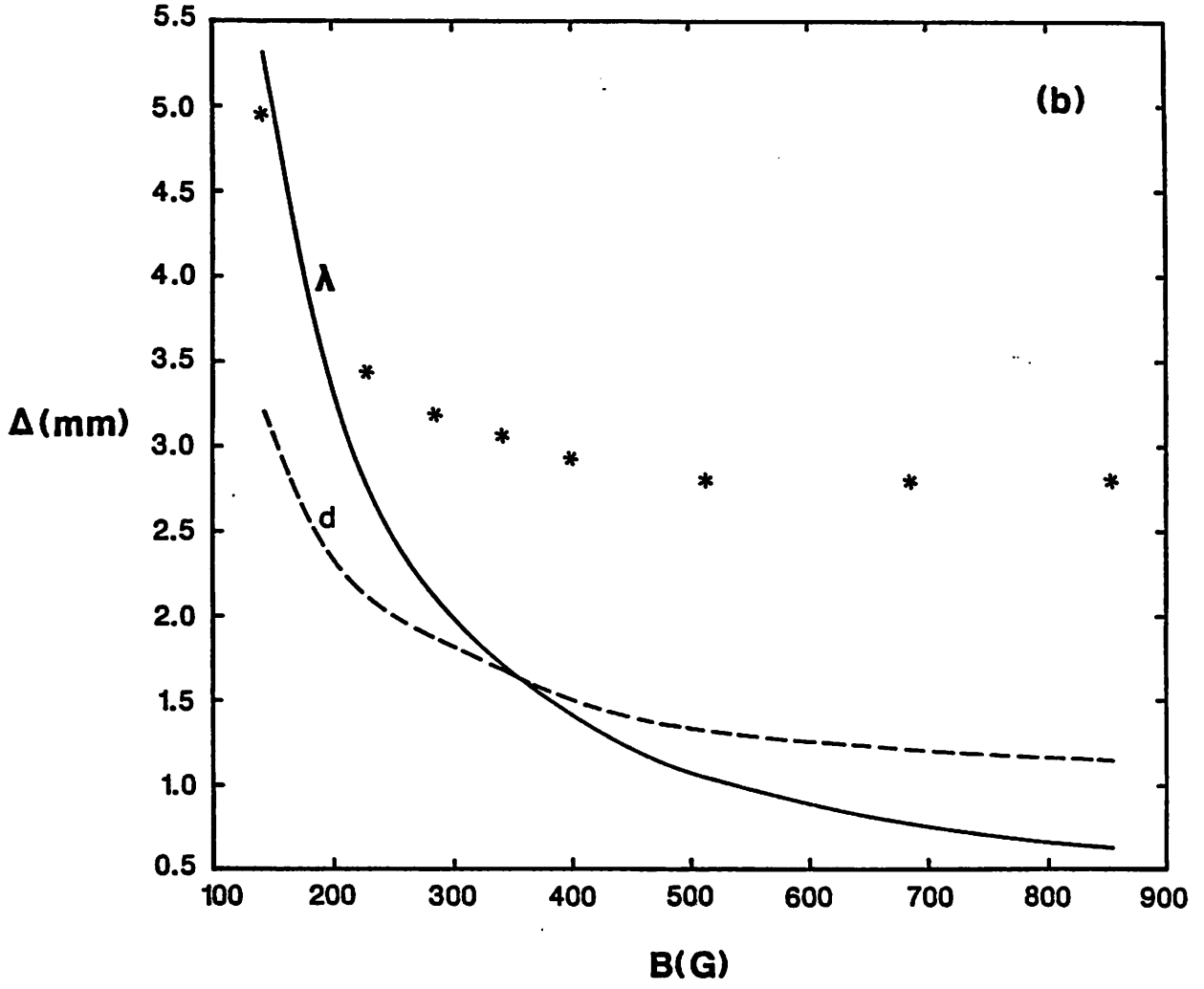
(b)
λ
d
Δ(mm)
B(G)
5.5
5.0
4.5
4.0
3.5
3.0
2.5
2.0
1.5
1.0
0.5
100
200
300
400
500
600
700
800
900

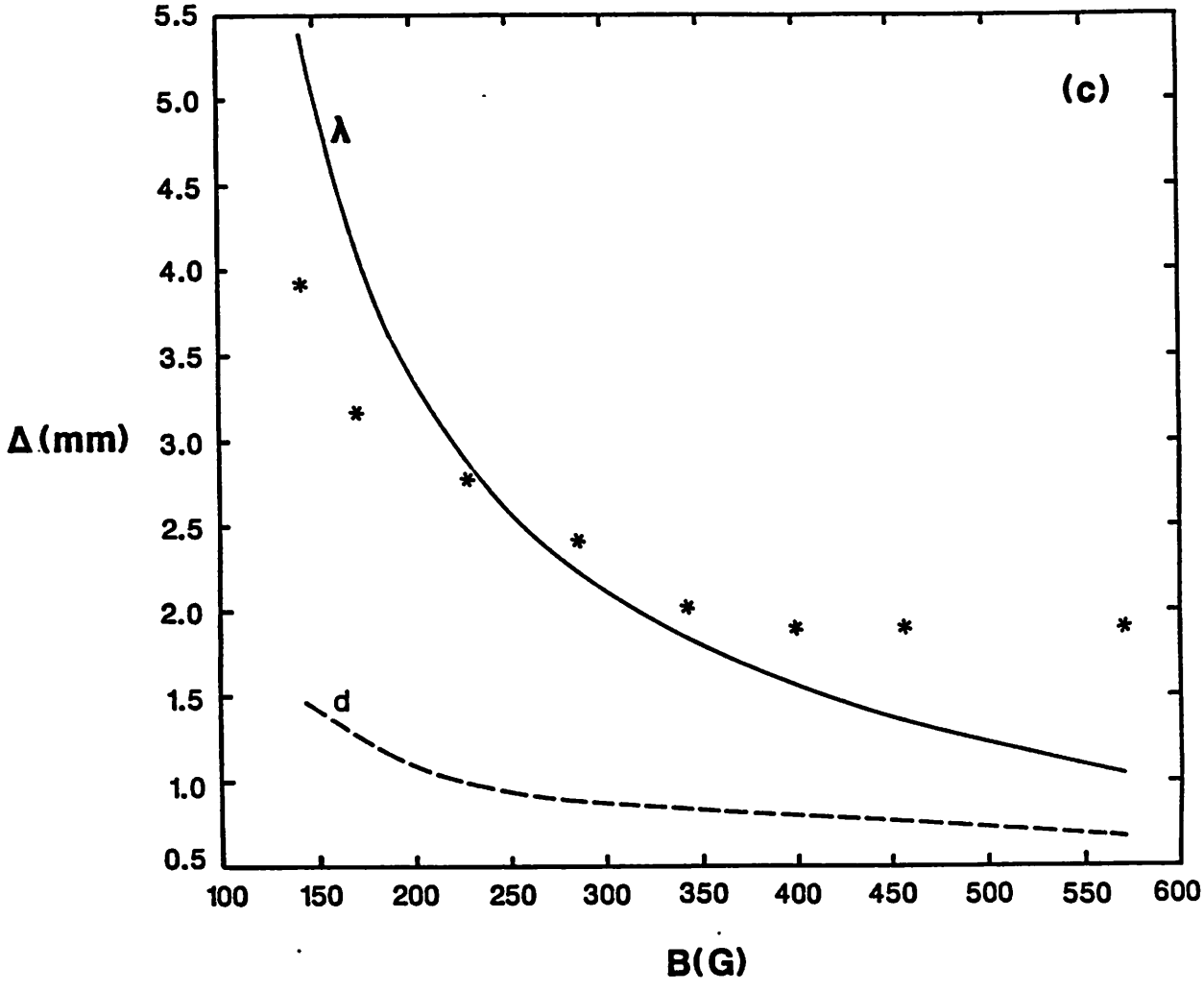
(c)
λ
d
Δ(mm)
B(G)
5.5
5.0
4.5
4.0
3.5
3.0
2.5
2.0
1.5
1.0
0.5
100
150
200
250
300
350
400
450
500
550
600

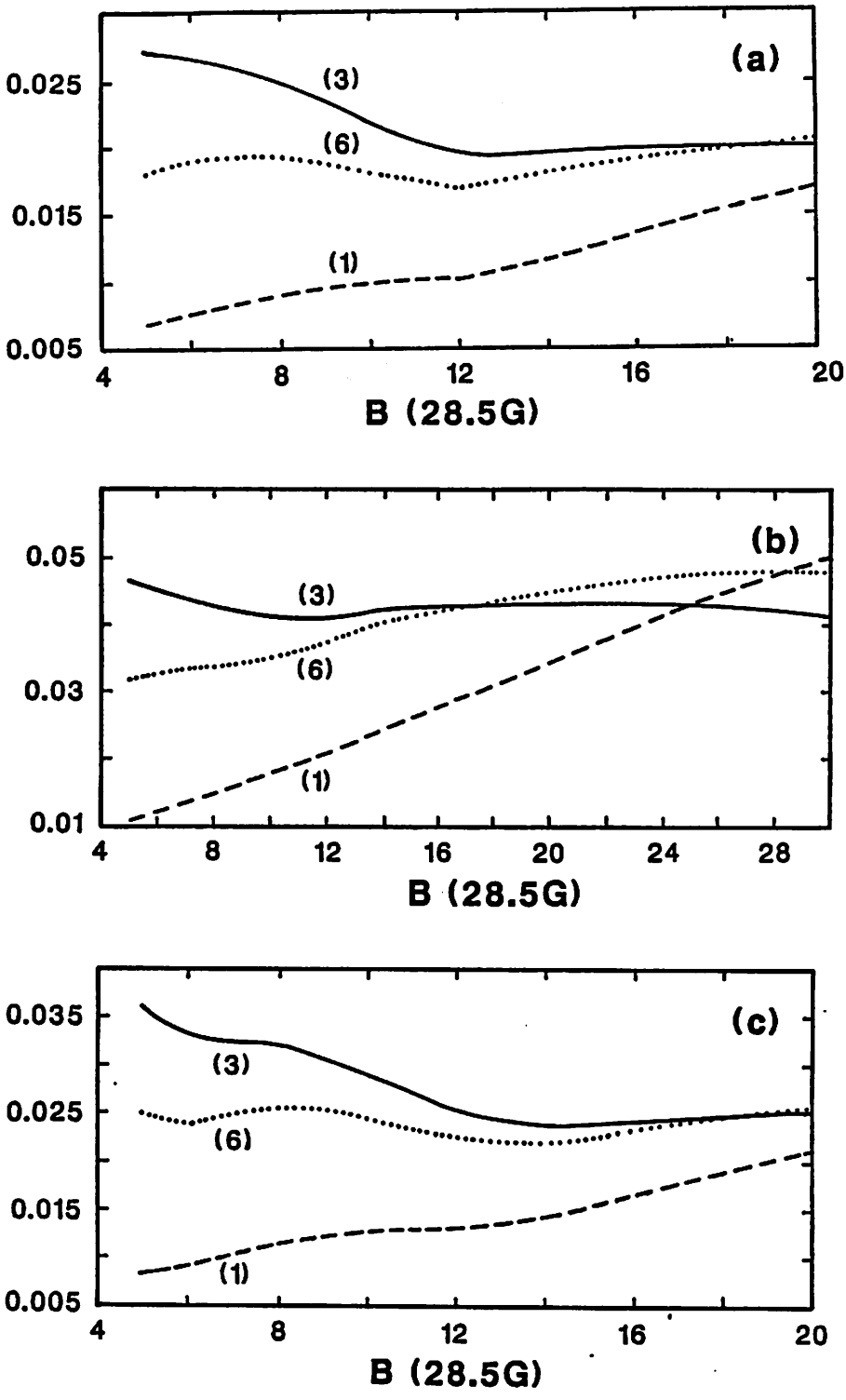

Fig. 7. Test of scaling laws [Eq. (1) Eq. (3), and Eq. (6)] for Δ; (a) I = 0.5 A, p = 5 mtorr; (b) I = 0.1 A, p= 5 mtorr; (c) I = 0.5 A, p = 20 mtorr.

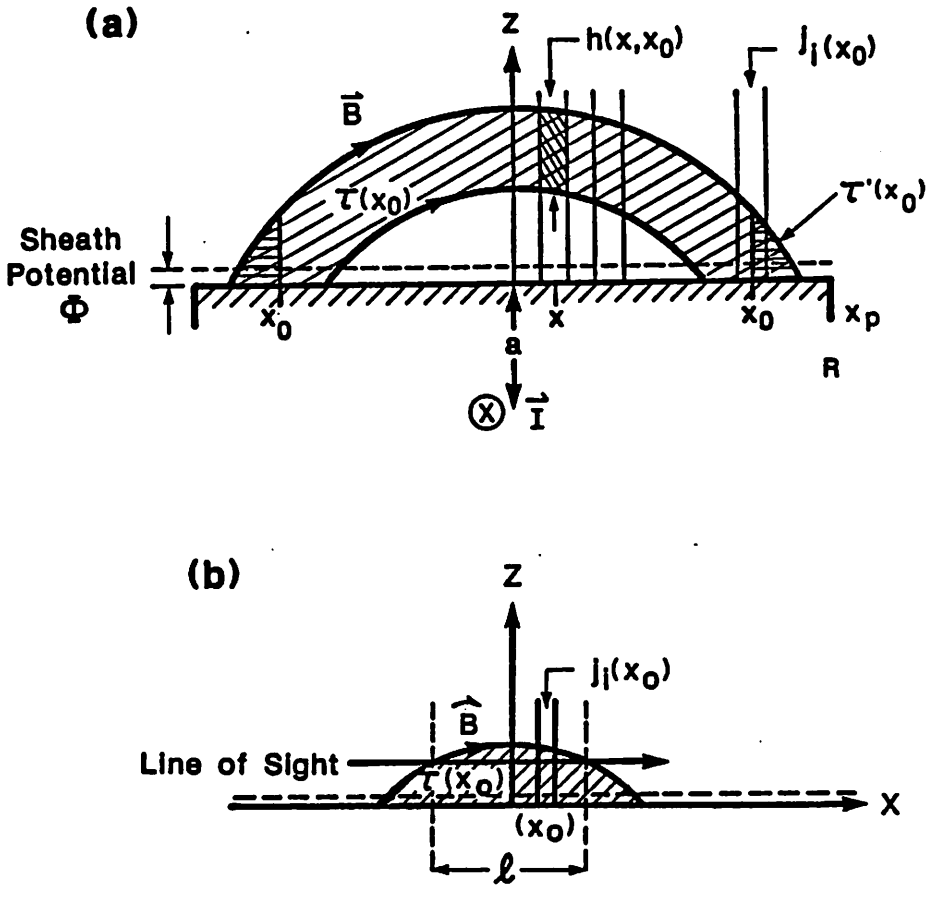

Fig. 8. Two dimensional, rectangular geometry model for current distribution at the cathode; (a) formulation of integral equation; (b) calculation of axially-resolved optical emission.

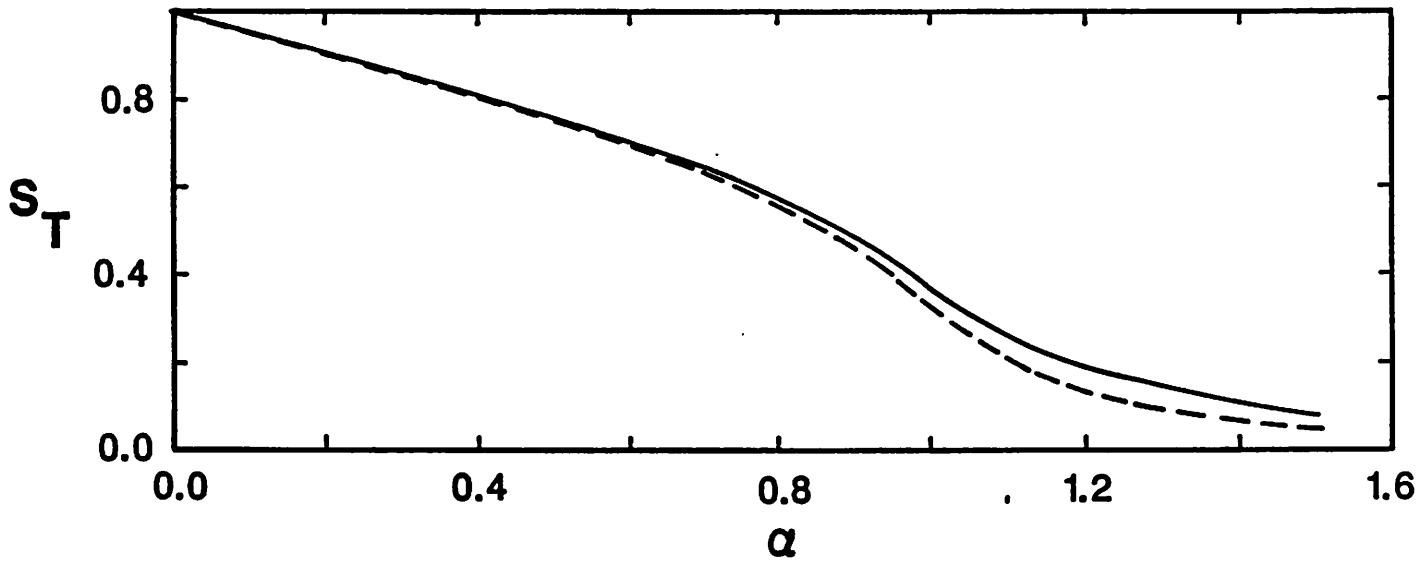

Fig. 9. Normalized optical emission S_T versus normalized axial position $\alpha = z/\overline{w}$. The solid curve is for a Gaussian profile; the dotted curve is for a rectangular profile.

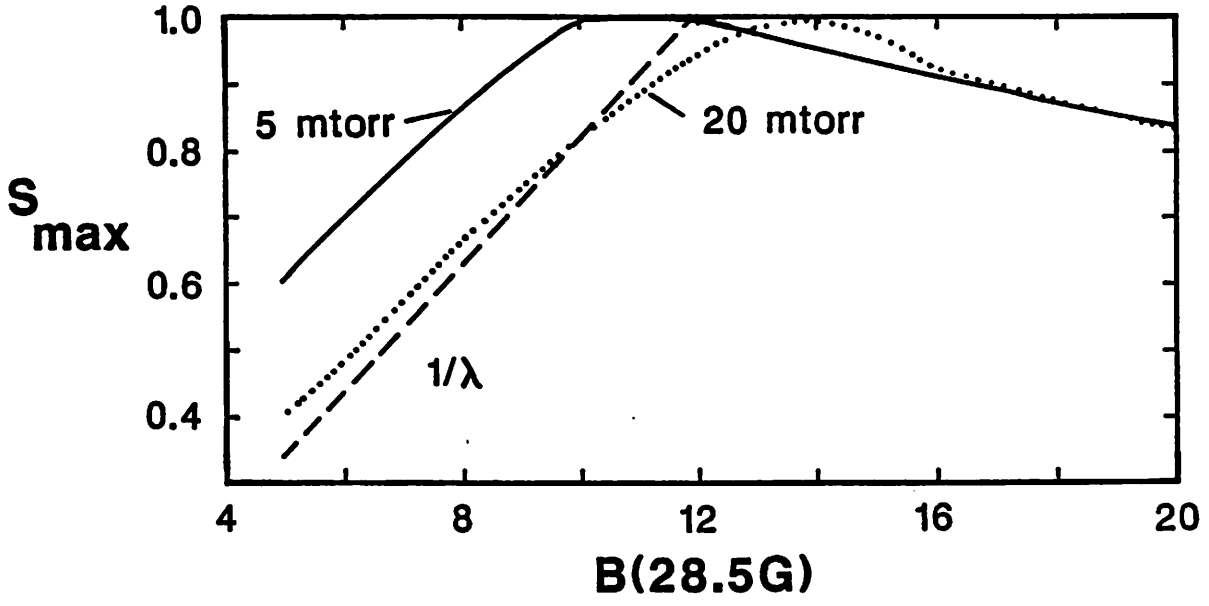

Fig. 10. Maximum value S_{max} (with respect to z) of the optical emission versus magnetic field B. The data for each pressure is normalized to its maximum with respect to B; I = 0.5 A. The predicted inverse gyroradius variation at low B is also shown.